RSC Applied Polymers

ROYAL SOCIETY OF CHEMISTRY

PAPER

View Article Online
View Journal | View Issue



Cite this: *RSC Appl. Polym.*, 2026, **4**, 298

# Benzoylation of microfibrillated cellulose–hydroxyapatite composites for green and water-resistant mechanical materials

Nana Taniguchi, Yui Mitsushima, Yui Okuda, Akuto Takagi, Eiichi Kido, Ken Hirota and Tadashi Mizutani *

If composite materials comparable to bone-like bioceramics can be produced on an industrial scale, it would be expected to contribute to carbon neutrality, reduce environmental pollution caused by waste, and promote the realization of a sustainable society. We prepared a composite of microfibrillated cellulose and hydroxyapatite (HAP) with a hydroxyapatite weight fraction of 52% by crystallization of hydroxyapatite in a dispersion of microfibrillated cellulose in alkaline water at 50 °C. To improve water resistance of the composite, the composite was benzoylated with vinyl benzoate at 50–150 °C in DMF. Infrared absorption spectroscopy revealed that benzoylation proceeded above 110 °C. The benzoylated composites were uniaxially pressed at 120 °C at 300 MPa for 5 min to obtain the compacts. A three-point bending test revealed that the composite benzoylated at 110 °C exhibited ductile fracture, with an elastic modulus of 4.5 ± 0.2 GPa and a bending strength of 65.7 ± 1.2 MPa. When the compacts were immersed in water at room temperature for 24 h, the water absorption ratios of the composite benzoylated at 50–100 °C were 20–40%, while those benzoylated at 110–150 °C were less than 10%. The composite benzoylated at 110 °C had an elastic modulus of 3.3 ± 0.4 GPa and a bending strength of 38.4 ± 1.1 MPa. In contrast to the benzoylated TEMPO-oxidized cellulose nanofibers–HAP composite previously reported, whose modulus decreased to 2% of its original value after water immersion, the present composite retained 73% of its initial modulus, indicating a substantial improvement in water resistance.

Received 10th September 2025,
Accepted 3rd November 2025

DOI: 10.1039/d5lp00282f

rsc.li/rscapplpolym



## Introduction

Consumption of petroleum-derived plastics has caused several environmental issues such as microplastic pollution in sea water[1] and greenhouse gas generation during waste incineration.[2,3] Development of $CO_2$ neutral and biodegradable alternatives of consumer plastics is urgently demanded. We have been inspired by environmentally benign, lightweight and tough bioceramics to develop green mechanical materials. Bones, for instance, consist of carbonated apatite, collagen, and water in a volume ratio of approximately 56–60 : 30–40 : 10.[4–6] A composite material exhibiting both rigidity and high toughness is formed through the binding of nano-sized apatite crystals (5 nm in thickness, 80 nm in width, and several hundred nanometers in length) with collagen fibers.[7] If we define the main component of a composite material as the matrix and the secondary component as the filler, conventional polymer–ceramic composites typically utilize the inorganic filler phase to enhance rigidity. In contrast, in bioceramics, the polymeric filler plays a crucial role in preventing brittle fracture. Furthermore, bioceramics contain numerous hydrophilic groups in both their organic and inorganic phases, with water playing an essential role in structural formation and mechanical functionality. Research in this area has only recently begun, and questions regarding which components to combine, how to integrate them, and in what proportions remain to be clarified in future studies. Since collagen, the organic component of bone, is prone to denaturation and difficult to obtain in large quantities, we have chosen cellulose—a biopolymer with a fibrous structure similar to that of collagen—as a substitute. Considering that cellulose is produced by photosynthesis in a large quantity ($10^{11}$–$10^{12}$ tons (ref. 8)) annually and utilization of cellulose can lead to preservation of wood resource on earth, the composite of cellulose and hydroxyapatite could adequately meet the demand as an alternative to plastics or even steel, and is expected to contribute to the realization of a sustainable society.[2,3,9–13]

The studies mimicking the outstanding mechanical properties of bioceramics—such as bones and teeth—revealed

*Department of Applied Chemistry, Faculty of Science and Engineering, Doshisha University, 1-3, Tatara-miyakotani, Kyotanabe, Kyoto 610-0394, Japan.*
*E-mail: tmizutan@mail.doshisha.ac.jp*

that the following factors affect the mechanical properties of the composite materials: (1) inorganic/organic weight ratios,[14] (2) water content,[5,15,16] particularly confined water molecules in-between apatite crystals and the organic phase (collagen fibers),[17,18] (3) the sizes of the organic phase and the inorganic phase, and their aspect ratios,[19] (4) orientation of fibrous structures of organic polymer and inorganic crystals, (5) binding of polymers to the surface of inorganic crystals,[20] and (6) charge distribution of the polymers and balance of hydrophilic and hydrophobic groups of the polymers.[21–23]

A number of investigations revealed that polymers with anionic functional groups concentrate calcium ions, assist nucleation of HAP crystals, and bind to the surface of HAP crystals *via* ionic interactions.[24–29] We reported that the cellulose derivatives having anionic functional groups such as carboxymethyl cellulose[30] and TEMPO-oxidized cellulose nanofibers (TCNF)[31] were hybridized with hydroxyapatite by coprecipitation, and the composites showed high rigidity, an elastic modulus of up to 7.7 GPa and a bending strength of 112 MPa.[30] When the molded composites of the anionic polymers and hydroxyapatite are immersed in water, however, they adsorbed a significant amount of water and cannot retain their shape, because the anionic functional groups are strongly hydrated and the surface of hydroxyapatite is also hydrophilic. The enhancement of water resistance of these composites represents the next challenge.

In the previous studies,[32,33] we revealed that acylation[34–39] of starch or TCNF in the composites with hydroxyapatite reduced the water absorption ratio of the densified compacts, and the water absorption ratio strongly influence the mechanical properties. The water absorption ratio can be governed by hydrophobicity of the polymer/apatite surfaces and the porosity of the molded compacts.

In this study, we report the development of water-resistant composite materials through benzoylation of microfibrillated cellulose (MFC)–HAP composites.[40] MFC[41] was selected as the organic polymer component for the following two reasons: (1) MFC lacks anionic groups and is therefore less hydrophilic than TCNF, which possesses anionic groups, making it more amenable to imparting water resistance; and (2) MFC–HAP composites do not undergo brittle fracture, leading to the expectation that their benzoylated counterparts would also exhibit high toughness. The water absorption ratio of the compact of the MFC–HAP composite was reduced to 5.4–10% by benzoylation, and the elastic modulus of the compacts immersed in water was 3.3 GPa while that was 4.5 GPa before immersion in water. Benzoylation of the MFC–HAP composite is effective for the development of environmentally friendly engineering materials that exhibit a combination of high rigidity, high toughness, water resistance, and low weight.

# Experimental

Microfibrillated cellulose (Celish KY100G, 10 wt% aqueous dispersion) was provided by Daicel Corporation, Japan. Vinyl benzoate was purchased from Tokyo Chemical Industry, Co., Ltd, Japan. Thermogravimetric and differential thermal analysis (TG-DTA) was performed with a Shimadzu DTA-60 thermogravimetric analyzer (Japan). Powder X-ray diffraction (XRD) of the composite powder was recorded on a Rigaku SmartLab diffractometer (Japan) with Cu-Kα radiation. Fourier transform infrared (FT-IR) spectra were recorded as KBr pellets on a JASCO FT/IR-4600 spectrophotometer (Japan). Scanning electron microscopy (SEM) observations and energy dispersive X-ray spectroscopy (EDS) were carried out either with a Hitachi High-technology SU8020 field emission scanning microscope (Japan) or with a Hitachi TM3030Plus microscope (Japan).

### Preparation of MFC–HAP composites

To a 10 wt% aqueous dispersion of MFC (23.3 g) was added 0.2 M $Na_2HPO_4$ (69.7 mL) and 1 M NaOH (18.6 mL), and the mixture was stirred at 50 °C for 30 min. Then, 0.2 M aqueous $CaCl_2$ (116 mL) was added dropwise at a rate of one drop per second, and the suspension was stirred at 50 °C for 1 h. After cooled to room temperature, acetone (253 mL) was added. White precipitates were collected with suction filtration. The precipitates were washed with acetone–water (1 : 1) (1 L), and then with acetone (2 L). The white powder was dried *in vacuo* at 80 °C for 2 h to quantitatively obtain 4.67 g of the composite.

### Benzoylation of MFC–HAP composites

The MFC–HAP composite (1.5 g) was mixed with vinyl benzoate (1.71 mL), $K_2CO_3$ (0.5 g) and *N*,*N*-dimethylformamide (DMF) (50 mL). The mixture was stirred at 50, 70, 100, 110, 130, and 150 °C for 4 h. After the reaction mixture was cooled to room temperature, MeOH (1 L) was added. The powder was collected by suction filtration and washed with MeOH (1 L) and then with water (1 L). The powder was dried *in vacuo* at 80 °C for 2 h.

### Inorganic contents of the composite

To determine inorganic contents (IC) of the composites, the composite powder was subjected to TG-DTA analysis. The sample was heated in an alumina pan in air from room temperature to 100 °C at a rate of 20 °C $min^{-1}$, kept at 100 °C for 10 min, heated to 1000 °C at a rate of 20 °C $min^{-1}$, and kept at 1000 °C for 10 min. The sample was cooled to 100 °C at a rate of 100 °C $min^{-1}$. The weight% of inorganic components was calculated as a ratio of the final weight to that at 100 °C in the first heating.

### Densification of the benzoylated MFC–HAP composite powder and three-point bending test

The benzoylated MFC–HAP composite powder was placed in a tungsten carbide mold of 4 mm × 13 mm, and uniaxially pressed at 300 MPa at 120 °C for 5 min to obtain the molded composites of 4 mm × 13 mm × 1.5–1.8 mm. The bulk density of the compacts ($d_{bulk}$) was determined from the ratio of the sample weight to the volume of the rectangular parallelepiped. A three point bending test was conducted immediately after the compression molding process. The load is applied to the

sample with a cross head speed of 0.5 mm min$^{-1}$. Stress $P$ was calculated by

$$P = \frac{3FL}{2wt^2},$$

where $F$ is the load (N), $L$ is the length between the supporting points (8 mm), $w$ is the breadth (4 mm) and $t$ is the thickness (1.5–1.8 mm) of the specimen. Strain $\varepsilon$ was calculated according to

$$\varepsilon = \frac{6ts}{L^2},$$

where $s$ (m) is the displacement of the cross-head. Bending elastic modulus, $E_b$, was calculated from the slope of the stress–strain line according to

$$E_b = \frac{\Delta P}{\Delta \varepsilon}.$$

The work of fracture[42] of the composite was measured by determining the area under the load ($F$)–displacement ($s$) curve and dividing by the area of the fracture surface. The mechanical properties were generally presented as the mean values and standard errors of the mean obtained from three to four measurements. In the case of samples with poor water resistance after water immersion, the data include those derived from two measurements.

### Water resistance test of the compacts

The compacts (4 mm × 13 mm × 1.5–1.8 mm) were immersed in distilled water at room temperature for 24 h. The molded specimen was removed, the surface water was wiped off with a Kimwipe, and the weight measurement and bending test were conducted immediately. The water absorption ratio, $(w_{wet} - w_{dry})/w_{dry}$, was calculated, where $w_{dry}$ and $w_{wet}$ is the weight of the compact before immersion in water and after immersion in water, respectively.

## Results and discussion

### Benzoylation of MFC–HAP composites

Composites of microfibrillated cellulose (MFC) and hydroxyapatite (HAP) with a feed ratio of 50 : 50 (wt/wt) were prepared according to the previously reported procedure.[40] TG-DTA of the MFC–HAP composite showed that the inorganic content was 52%. The compact of the composite is light weight (density of 1.6 g cm$^{-3}$), with a bending strength of 97 MPa and an elastic modulus of 8.0 GPa. The bending strength was similar to that of engineering plastics and the elastic modulus was greater than that of engineering plastics. However, the compact adsorbed a significant amount of water upon immersion in water, resulting in a loss of rigidity. Collagen, a major organic component of bone, contains 31 mol% of hydrophobic amino acids (Ala, Val, Leu, Ile, Pro and Phe), 7.5 mol% of cationic amino acids (Arg and Lys), and 11.9 mol% of anionic amino acids (Asp and Glu).[43] Therefore, hydrophilic/hydrophobic balance of the polymer should be an important factor affecting the water sensitivity of the composite. There are two possible approaches to impart water resistance to the composite: (1) introduction of hydrophobic moieties to the composite, and (2) introduction of polar functional groups on cellulose surface to stabilize the interface between cellulose and HAP. In this study, we attempted to introduce hydrophobic acyl groups to cellulose to improve water resistance of the MFC–HAP composite. In our previous research on acylation of cellulose nanofibers–HAP composites,[33] we found that variations in the acyl group structure affect not only the water resistance but also rigidity of the composites. The acylation of the cellulose nanofibers–HAP composites resulted in a decrease in the elastic modulus to 70% (acetyl), 59% (hexanoyl), 40% (octanoyl), 42% (lauroyl), and 70% (benzoyl) of its original value.[33] Since the acetylated composites exhibited poor water resistance, the benzoyl group is a promising acyl group for imparting water resistance to the composite without compromising its rigidity.

Benzoylation of the hydroxy groups of cellulose in the composites were performed in DMF using vinyl benzoate and potassium carbonate over a temperature range of 50 to 150 °C for 4 h (Scheme 1). We employed vinyl benzoate as a benzoylation reagent. Use of benzoyl chloride or benzoic anhydride generate hydrochloric acid or benzoic acid as a by-product during the reaction and acid-sensitive hydroxyapatite crystals could be decomposed. Benzoylation with vinyl benzoate yields volatile acetaldehyde as a by-product. It does not induce the decomposition of hydroxyapatite crystals. The progress of the reaction was monitored by infra-red spectroscopy. The ester carbonyl stretching band appeared at 1730 cm$^{-1}$ when the benzoylation temperature was higher than 100 °C (Fig. 1). The composites benzoylated within the temperature range of 110 °C and 150 °C exhibited new peaks at 1273 and 710 cm$^{-1}$. The former peak is assigned to antisymmetric stretching of the ester C–O–C group and the latter peak is assigned to C–H out-of-plane bending vibration of mono-substituted benzene, a character-

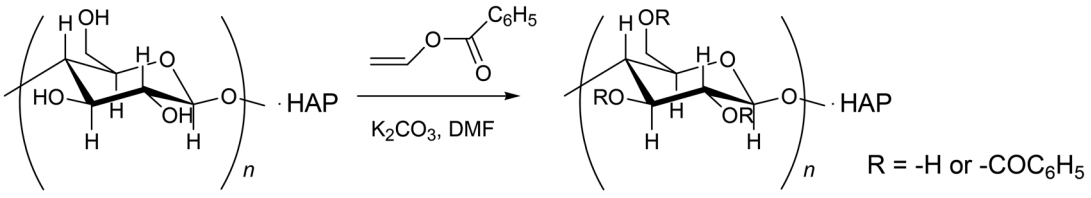


Scheme 1 Benzoylation of MFC–HAP composites.

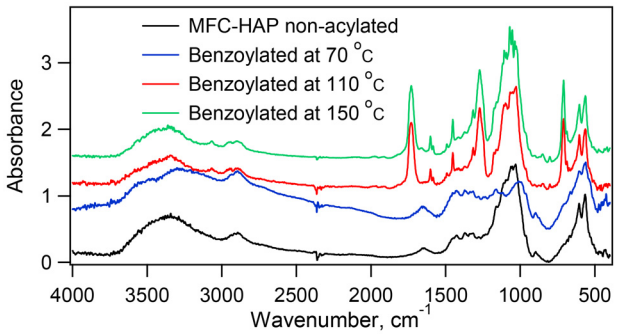


**Fig. 1** Infra-red spectra of the MFC–HAP composite and the benzoylated MFC–HAP composites.

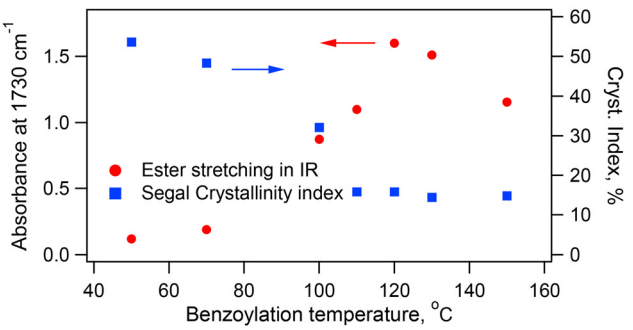


**Fig. 2** Absorbance of the ester carbonyl stretching vibration of IR and the Segal crystallinity index of cellulose of the benzoylated composites *versus* benzoylation temperature.

istic peak of benzoyl ester.[44] Fig. 2 shows the plot of absorbance at the ester C═O stretching band against the benzoylation temperatures. The absorbance was normalized for the phosphate peak of HAP at 563 $cm^{-1}$. The absorbances increased as the reaction temperature was raised; however, it reached a plateau at temperatures exceeding 110 °C. These IR studies demonstrated that benzoylation proceeded when the reaction temperature was higher than 110 °C.

Benzoylation was carried out using DMF as the solvent. Preliminary studies on the reaction solvent confirmed that benzoylation also proceeded in DMSO; however, in nonpolar solvents such as toluene, the reaction did not progress sufficiently. As shown in Fig. S2 and S3, when the reaction temperature was increased to 100 °C and 130 °C, the white MFC–HAP composite became discolored, turning brown to black. Therefore, milder reaction conditions are desirable, and investigations on the choice of solvent, acylating agent, and catalyst are currently in progress.

Inorganic contents (IC) of the composites were determined from the TG traces (Fig. S1) and listed in Table 1. From the IC values, we estimated the degree of substitution, $x$, of the composite. We assumed the empirical formula of the composite, $C_6H_7O_2(OH)_{3-x}(OCOC_6H_5)_x{\cdot}\alpha Ca_{10}(PO_4)_6(OH)_2$, where $x$ is the degree of substitution, and $\alpha$ is determined by the IC value of

**Table 1** Inorganic contents and the degree of substitution of the composites

| Benzoylation temperature, °C | IC, % | Degree of substitution, $x$ |
|---|---|---|
| [a] | 51.6 | 0 |
| 50 | 50.8 | 0.05 |
| 70 | 51.6 | 0 |
| 100 | 44.1 | 0.54 |
| 110 | 37.5 | 1.21 |
| 120 | 35.7 | 1.43 |
| 130 | 38.1 | 1.14 |
| 150 | 39.5 | 0.99 |

[a] Before benzoylation.

the composite before benzoylation. The degree of substitution $x$ was calculated according to

$$x = \frac{1}{FW[C_7H_4O]}\left\{\alpha FW[Ca_{10}(PO_4)_6(OH)_2]\frac{1-IC}{IC} - FW[C_6H_{10}O_5]\right\},$$

where FW[$X$] represents the formula weight of $X$. The value of $\alpha$ is determined to be 0.172 by substituting $x$ = 0 and IC = 0.516 to the above equation. We assume that the value of $\alpha$ does not change upon benzoylation. The degree of substitution increased with increasing reaction temperature but became constant at 1.0–1.4 once it exceeded 110 °C (Table 1).

X-ray diffraction patterns of the composite powder are shown in Fig. 3. The XRD patterns of the composite before benzoylation indicated that the composite consists of nanocrystals of hydroxyapatite and cellulose $I_\beta$ crystals. The nanocrystalline structure of hydroxyapatite remained unchanged by benzoylation, whereas the diffraction peaks at $2\theta$ = 14.7, 16.4 and 22.6° corresponding to the cellulose $I_\beta$ crystal phase[45] decreased, indicating that benzoylation occurs not only on the crystal surface of cellulose but also inside the crystals. The crystallinity of cellulose was estimated from the Segal crystallinity index,[46] and shown in Fig. 2. The Segal crystallinity index decreased when the benzoylation temperature was higher than 100 °C. However, as discussed in the section on mechanical properties, the decrease in the crystallinity of cellulose did not

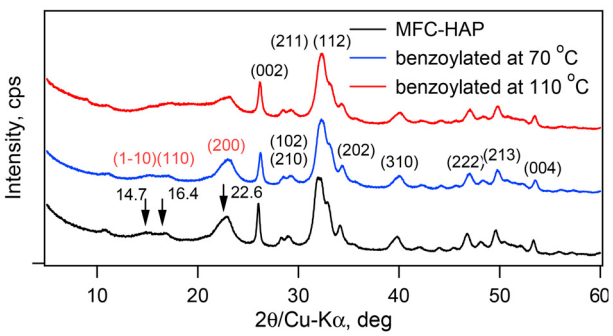


**Fig. 3** XRD patterns of the parent MFC–HAP composite and the benzoylated MFC–HAP composites. The indices of the diffraction peaks of HAP and those of cellulose $I_\beta$ are shown in black and red, respectively.

lead to a transition to brittle fracture, nor did it result in a reduction in toughness.

It is interesting to compare the benzoylation conditions with those of other polysaccharide–HAP composites. Benzoylation of tapioca starch–HAP composites with IC 45% and IC 66% proceeded at 60 °C and 80 °C, respectively, in DMSO.[32] Benzoylation of TCNF with IC 62% proceeded at 100 °C in DMSO.[33] Although DMF was used as a solvent in the present study, benzoylation of MFC–HAP composites with IC 52% required higher temperatures of 110–120 °C than benzoylation of starch–HAP composites. It is considered that the requirement for the higher temperature in the benzoylation of the MFC–HAP composite arises from the fact that the reaction occurs in a heterogeneous system containing solid and is accompanied by the degradation of cellulose crystals.

### Densification of benzoylated MFC–HAP composites and their mechanical properties

The composite powder of benzoylated MFC–HAP was densified uniaxially in a tungsten carbide mold at 120 °C at 300 MPa for 5 min. Fig. 4 shows the density of the compacts. The density of the compacts decreased from 1.75 to 1.6 g $cm^{-3}$ when the benzoyl groups were introduced to the composite.

The mechanical properties were evaluated by three-point bending test. Elastic modulus of the compacts of the MFC–HAP composite before benzoylation was 7.4 ± 0.3 GPa. The compacts benzoylated at 110–150 °C showed lower elastic moduli of 4.3–4.8 GPa (Fig. 4). The benzoyl moiety introduced on cellulose would break the intermolecular hydrogen bonds of cellulose, and also weaken the attractive interaction between cellulose and the HAP crystals, thereby weakening the rigidity of the compacts.

The elastic modulus of the composite decreased to 58–65% compared to the untreated one. In comparison to the previously reported case,[33] where the elastic modulus of TCNF–HAP composite decreased to 70% upon benzoylation, the reduction in elastic modulus observed in this study was more significant. However, the elastic modulus of the sufficiently benzoylated composites (4.3–4.8 GPa) is significantly higher than that of polyamide 66 (2.4–2.8 GPa, Table 2), indicating that the composites retain a high degree of rigidity even after benzoylation. Fig. 5 shows the plot of the bending strengths and the strains at failure against benzoylation temperature. It was found that benzoylation of the composite did not significantly alter its bending strength or strain at break.

Fig. 6 and S4 shows SEM images of the fracture surfaces obtained from the bending tests. A rough fracture surfaces were observed owing to the fibrous structure of cellulose. During the bending test, the specimen did not separate into two parts at the maximum load, indicating a ductile fracture. Although XRD analysis revealed that the crystallinity of cellulose decreased upon benzoylation, the occurrence of ductile rather than brittle fracture suggests that the fibrous structure, rather than the crystalline structure of cellulose, plays a crucial role in imparting toughness. In terms of fracture energy, which serves as an indicator of toughness, the complexes benzoylated below 100 °C exhibited the work of fracture of 320–400 J $m^{-2}$, whereas those benzoylated above 110 °C

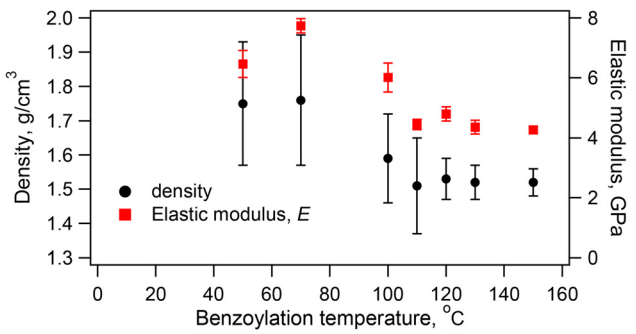


Fig. 4 Plot of the densities and elastic moduli, $E_b$, of the compacts of benzoylated composites against benzoylation temperatures. The standard errors obtained from three to four measurements were represented by error bars.

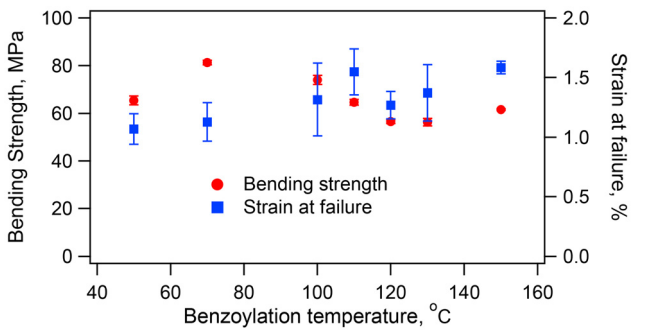


Fig. 5 Plot of bending strengths and strains at failure of benzoylated composites against benzoylation temperatures. The standard errors obtained from three to four measurements were represented by error bars.

Table 2 Comparison of the elastic moduli, $E$, and the bending or tensile strength, $\sigma$, of the benzoylated MFC–HAP composite[a] and polyamide 6,6

| | $E_{dry}$, GPa | $E_{wet}$, GPa | $E_{wet}/E_{dry}$, % | $\sigma_{dry}$, MPa | $\sigma_{wet}$, MPa | $\sigma_{wet}/\sigma_{dry}$, % | Ref. |
|---|---|---|---|---|---|---|---|
| Benzoylated MFC–HAP | 4.5 | 3.3 | 73 | 65 | 38 | 58 | This work |
| Polyamide 66 | 2.83 | 1.21[b] | 43 | 117 | 42[b] | 36 | 47 |
| | | 0.48[c] | 17 | | | | |
| Polyamide 66 | 2.4 | 0.5[d] | 21 | 92 | 33[d] | 36 | 48 |

[a] Benzoylated at 110 °C. [b] Relative humidity 50%. [c] Relative humidity 100%. [d] Immersed in water for 3 days at 80 °C.

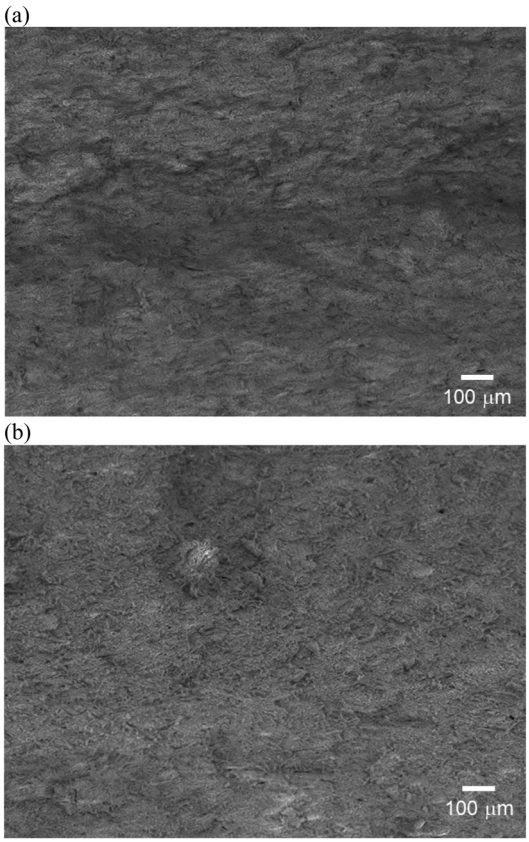


Fig. 6 SEM images of the fracture surfaces after the bending tests of the molded composites benzoylated at 130 °C, before (a) and after water immersion (b).

showed values of 310–410 J $m^{-2}$ (Table S1), indicating that benzoylation caused little reduction in toughness.

A summary of the fracture behaviors of various polysaccharide–hydroxyapatite composites reported so far is as follows: starch–hydroxyapatite[49] and carboxymethyl cellulose–hydroxyapatite composites[30] exhibit brittle fracture; the TEMPO-oxidized cellulose nanofiber (TCNF)–hydroxyapatite composite[31] shows brittle fracture when hydroxyapatite crystals formed on the well-dispersed TCNF, but ductile fracture when hydroxyapatite crystals formed on the aggregated TCNF; the microfibrillated cellulose (MFC)–hydroxyapatite composite exhibits ductile fracture, and its benzoylated counterpart also demonstrates ductile fracture. The composite composed of non-associated polymers exhibited brittle fracture, whereas the composite composed of polymers associated in a fibrous manner exhibited ductile fracture. Based on these considerations, if benzoylation of the MFC–HAP composite completely disrupted the crystalline structure of cellulose and rendered it fully amorphous, the molded bodies would likely exhibit brittle fracture. However, since the X-ray diffraction patterns (Fig. 3) retain a peak in the range of $2\theta$ = 15–25°, the fibrous structure of cellulose appears to be preserved, leading to ductile fracture of the molded bodies.

### Effects of water on the mechanical properties of the compacts

The compacts were immersed in distilled water at room temperature for 24 h, and the water absorption ratio was calculated by $(w_{wet} - w_{dry})/w_{dry}$, where $w_{dry}$ and $w_{wet}$ are the weight of the compact before and after immersion, respectively. The water absorption ratio was over 20% for the compacts benzoylated at 50, 70 and 100 °C, while it was 5.4–10% for the compacts benzoylated at 110–150 °C (Fig. 7 and Table S3). Fig. S2 shows a photograph of the molded composite, benzoylated at 100 °C, after being immersed in water at room temperature for 24 h. Cracks were observed in the molded composite. As shown in the photograph in Fig. S3, the molded composites, benzoylated at temperatures above 110 °C, exhibited no cracking after immersion in water and retained their original shape. The water absorption ratio of 5.4–10% was markedly lower than the 28% observed for the benzoylated TCNF–HAP composite (IC 62%).[33] This difference is presumed to arise from the abundance of carboxylate groups in TCNF. Bone, a composite of collagen and carbonated apatite, contains *ca.* 10% water, and the water endows bone with toughness. The fact that the water absorption ratio of the composite was between 5–10%, which is close to that of bone, is of particular interest.

The changes in the mechanical properties were determined by the three-point bending test (Table S2). The ratios of the elastic moduli of the wet compacts to those of the dry compacts, $E_{wet}/E_{dry}$, were smaller than 10% for the compacts benzoylated at 50–100 °C, while those were *ca.* 70% for the compacts benzoylated at 110–150 °C (Fig. 7). In the benzoylated TCNF–HAP, the $E_{wet}/E_{dry}$ ratio was 2%,[33] indicating that the benzoylated MFC–HAP exhibited substantially higher water resistance. The observation indicates that the water absorption ratio below 10% lead to water-resistant compacts. Nyman *et al.*[50] reported that the elastic modulus of wet human femurs is 10.8 GPa, and it is 15.5 GPa when dried. The ratio of the elastic modulus of wet human femurs to that of dry ones is also 70%.

Fig. 8 shows the ratios of the bending strengths of the compacts before and after immersion in water. For the composites

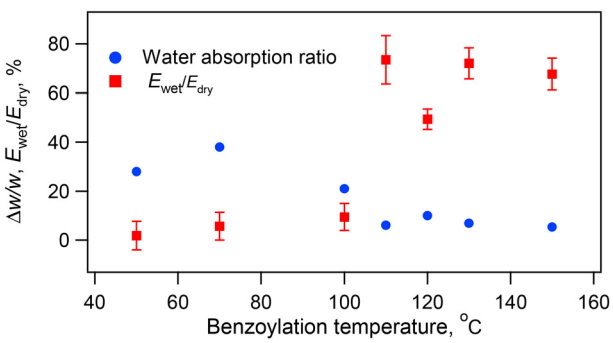


Fig. 7 Plot of the water absorption ratios, $\Delta w/w$, and the ratios of the elastic moduli, $E_{wet}/E_{dry}$, of the benzoylated composite compacts against benzoylation temperatures. The standard errors obtained from three to four measurements were represented by error bars.

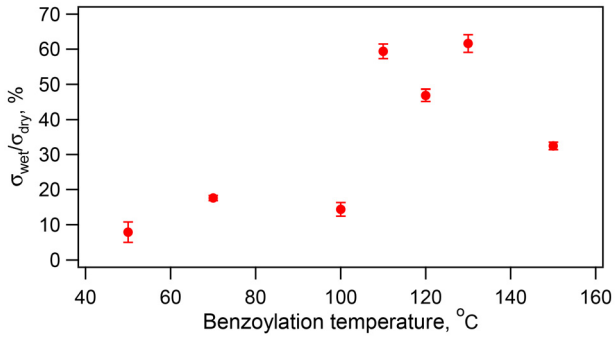


**Fig. 8** Plot of the ratios of bending strengths of the wet compacts to those of the dry compacts ($\sigma_{wet}/\sigma_{dry}$) against benzoylation temperatures. The standard errors obtained from three to four measurements were represented by error bars.

benzoylated below 100 °C, the bending strength of the compacts immersed in water was reduced to 20% of the dry ones, indicating that the compacts were not water-resistant. In contrast, for the composites benzoylated above 110 °C, the bending strength of the compacts immersed in water were 50–70% of that of the dry ones. These results demonstrated that benzoylation at sufficient temperatures improved both rigidity and strength of the compacts. Even when the benzoylation temperature was increased from 110 to 150 °C, the mechanical properties and water resistance of the composites did not significantly change. Considering that the color of the products darkened from brown to black with increasing reaction temperature, performing the benzoylation at 110 °C is considered to be the most appropriate.

Fig. 6 shows SEM images of the fracture surfaces after the bending tests of the molded composites benzoylated at 130 °C, before and after water immersion. A fiber structure with a diameter of approximately 5 μm and a length of about 100 μm was observed particularly on the fracture surface of the molded compact after water immersion. In the bending tests, the molded compacts before and after water immersion did not separate into two pieces but fractured while remaining connected. The fracture surfaces were exposed by manually pulling the molded compacts apart for SEM observation.

The molar fractions of calcium, phosphorus, and carbon atoms on the fracture surface were found to be in close agreement with those calculated from the inorganic weight fraction (see Table S4). However, the molar fractions of calcium and phosphorus were slightly lower, while that of carbon was slightly higher. These results suggest that cellulose is preferentially exposed on the fracture surface rather than hydroxyapatite.

### Comparison of mechanical properties and water absorption ratio for acylated starch–HAP, TCNF–HAP and MFC–HAP composites

The effect of water absorption on the mechanical properties of the composites was compared among acylated composites of starch–HAP,[32] TCNF–HAP,[33] and MFC–HAP. The acyl groups were benzoyl and lauroyl for starch, acetyl, hexanoyl, octanoyl, lauroyl, and benzoyl for TCNF, and benzoyl for MFC. All of these samples were synthesized using nearly the same procedure and molded at 300 MPa for MFC–HAP and TCNF–HAP composites and at 120 MPa for starch–HAP composites. The benzoylated polysaccharide–HAP composites exhibiting the highest $E_{wet}/E_{dry}$ ratio were selected and their mechanical properties in the dry state and after water immersion were compared in Table 3. Fig. 9 shows the plot of the relative elastic moduli, $E_{wet}/E_{dry}$, and the relative bending strengths, $\sigma_{wet}/\sigma_{dry}$, against the volume fraction of water. Composites that absorbed more than 15% water exhibited a reduction both in elastic modulus and bending strength to less than 20% of the original value, whereas composites that absorbed less than 10% water retained more than 50% of the original modulus and 30% of the original strength after immersion in water. Data for acetylated starch–HAP composites were omitted in the plot, since they exhibited small values of $E_{wet}/E_{dry}$ and $\sigma_{wet}/\sigma_{dry}$ even if water absorption ratios were smaller than 10%. The points marked with * in Fig. 9(a) also showed small values of $E_{wet}/E_{dry}$. These points represent lauroylated starch–HAP, and lauroylation caused significant reduction in elastic moduli in the dry state. These results demonstrate that there is a strong correlation between the water absorption ratios and rigidity. Based on the $E_{wet}/E_{dry}$ values and the $\sigma_{wet}/\sigma_{dry}$ values shown in Fig. 9, it was found that the water resistance of the composites decreases in the order acylated starch–HAP ~ acylated MFC–HAP > acylated TCNF–HAP. The low water resistance of the acylated TCNF–HAP composite is presumably attributable to the abundance of carboxylate groups in TCNF. The acylated starch–HAP composite undergoes brittle fracture and exhibits a smooth fracture surface, whereas the acylated MFC–HAP composite and the acylated TCNF–HAP composite do not frac-

**Table 3** Comparison of the elastic moduli ($E$), the bending strength ($\sigma$), and the strains at failure ($\varepsilon$) of the benzoylated polysaccharide–HAP composites[a]

| | Benzoylated MFC–HAP[c] | Benzoylated starch–HAP[32] | Benzoylated TCNF–HAP[33] |
|---|---|---|---|
| IC, % | 37.5 | 25 | 53 |
| $E_{dry}$, GPa | 4.50 ± 0.17 | 2.08 ± 0.08 | 8.1 ± 0.1 |
| $E_{wet}$, GPa | 3.3 ± 0.4 | 1.65 ± 0.08 | 0.17 ± 0.04 |
| $E_{wet}/E_{dry}$, % | 73 ± 12 | 79 ± 7 | 2.1 ± 0.6 |
| $\sigma_{dry}$, MPa | 65.7 ± 1.2 | 30.9 ± 0.8 | 64 ± 2 |
| $\sigma_{wet}$, MPa | 38.4 ± 1.1 | 19.2 ± 0.4 | 4.9 ± 0.4 |
| $\sigma_{wet}/\sigma_{dry}$, % | 59 ± 3 | 62 ± 3 | 7.7 ± 0.9 |
| $\varepsilon_{dry}$, % | 1.5 ± 0.2 | 2.5 ± 0.07 | 0.82 ± 0.04 |
| $\varepsilon_{wet}$, % | 1.3 ± 0.2 | 1.7 ± 0.2 | 3.0 ± 0.4 |
| $\varepsilon_{dry}/\varepsilon_{dry}$, % | 89 ± 3 | 68 ± 10 | 370 ± 70 |
| Fracture mode[b] | Ductile | Brittle | Ductile |

[a] The standard errors of the mean with 3 to 4 independent determinations are shown. [b] Brittle fracture: the molded specimen separated into two parts at the maximum load and the fracture surface was smooth, ductile fracture: the molded specimen did not separate into two parts at the maximum load, and the fracture surface was rough. [c] Benzoylated at 110 °C.

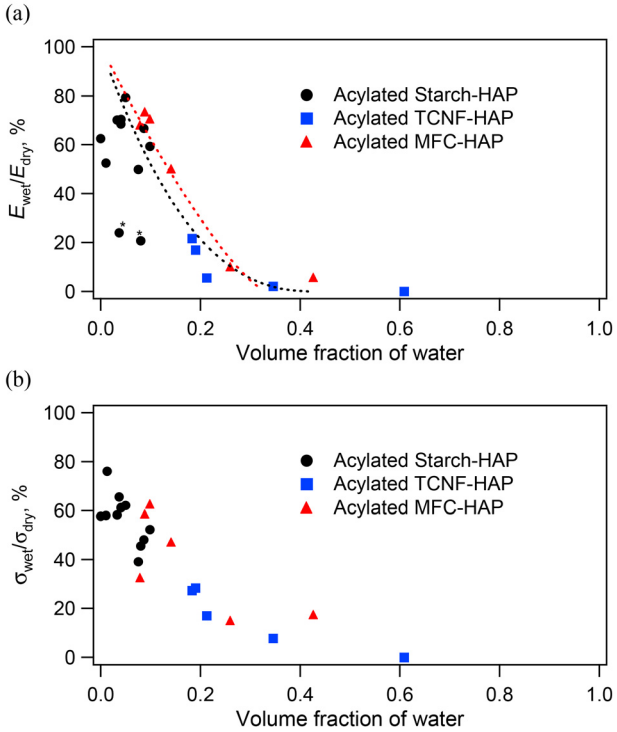


**Fig. 9** Plots of the relative elastic moduli, $E_{wet}/E_{dry}$ (a) and the relative bending strengths, $\sigma_{wet}/\sigma_{dry}$ (b) against the volume fraction of water for acylated starch–HAP composites,[32] acylated TCNF–HAP composites,[33] and benzoylated MFC–HAP composites. Least-squares fitting of all the data and the data of benzoylated MFC–HAP to $E_{wet}/E_{dry} = (1 - a\phi)^n$, where $\phi$ is the volume fraction of water, are shown in black dotted line and red dotted line, respectively.

ture even at maximum stress, and their fracture surface reveals a fibrous structure.

Table 2 compares the mechanical properties of benzoylated MFC–HAP composites and polyamide 66 in both dry and wet conditions. The ratios of $E_{wet}/E_{dry}$ and $\sigma_{wet}/\sigma_{dry}$ of benzoylated MFC–HAP were both larger than those of polyamide 66, indicating that the benzoylated MFC–HAP composite exhibited superior water resistance compared to polyamide 66. The elastic modulus of the benzoylated MFC–HAP composite after water immersion was 3.3 ± 0.4 GPa, which is higher than that of polyamide 66 after water immersion (0.5–1.2 GPa), indicating the potential applicability of this composite as an alternative to polyamide 66.

### Relationship between elastic modulus and water absorption

Relationship between elastic modulus and porosity of solids has been studied recently.[51] Phani showed that the expression $E = E_0(1 - aP)^n$, where $E$ is the elastic modulus at porosity $P$, and $a$ and $n$ are material constants related to the packing geometry and pore structure of the materials, respectively, can describe the interrelation of Young's modulus and porosity in porous brittle solids.[52] On the basis of this formalism, we considered that elastic modulus of the wet composite can be calculated by treating water as porosity according to the following equation:

$$\frac{E_{wet}}{E_{dry}} = \begin{cases} (1 - a\phi)^n & \text{if} \quad \phi < 1/a \\ 0 & \text{if} \quad \phi > 1/a \end{cases}$$

where $\phi$ is the volume fraction of water. According to the percolation theory, $1/a$ is the critical volume fraction of water at which a solid phase forms a continual network spanning the whole system.[53] The volume fraction $\phi$ was obtained from the following equation,

$$\phi = \frac{\frac{\Delta w}{w} d}{1 + \frac{\Delta w}{w}}$$

where $\Delta w/w$ is the water absorption ratio, $d$ is the density of the compact after immersion in water. By applying least-squares fitting to the data shown in Fig. 9(a), values of $a$ and $n$ were determined to be 2.3 and 2.5, respectively. The black dotted line shown in Fig. 9(a) is calculated with these parameters. When the fitting was performed using only the data for the benzoylated MFC–HAP composites, values of $a$ = 3.0 ± 0.5, $n$ = 1.3 ± 0.4 were obtained, and the calculated line is shown in the red dotted line in Fig. 9(a) (see also Fig. S6). It was found that the threshold volume fraction of water of the benzoylated MFC–HAP compacts at which the molded compact lost its rigidity was 0.33.

The relationship between the volume fraction of water and the elastic modulus has been clarified. However, it is still necessary to determine where water is adsorbed within the composite moldings. Water is likely adsorbed between cellulose fibers, between composite particles, and at the interfaces between cellulose and HAP. Clarifying these aspects would contribute to the rational design of composite materials inspired by bioceramics containing water.

## Conclusions

The composites of microfibrillated cellulose and hydroxyapatite were prepared by crystallization of HAP in an alkaline aqueous dispersion of MFC. To improve water resistance, the composite powder was benzoylated with vinyl benzoate in DMF. Infra-red and thermogravimetric studies indicated that a sufficient degree of benzoyl substitution was achieved in the cellulose at temperatures above 110 °C. X-ray diffraction showed that crystallinity of cellulose was reduced upon benzoylation, but SEM observation of the fracture surface showed there is a fibrous structure on the surface to result in ductile fracture. When the MFC–HAP compacts before benzoylation were immersed in water at room temperature for 24 h, they adsorbed a significant amount of water, resulting in a loss in rigidity. Benzoylation above 110 °C reduced the water absorption ratio to as low as 5–10%. The elastic modulus of the benzoylated MFC–HAP compacts immersed in water at room temperature for 24 h was *ca.* 70% of that of the dry compacts, indicating that the compacts were water-resistant and

can be used as rigid materials under humid or wet conditions. The elastic modulus of the benzoylated MFC–HAP composite after water immersion was 3.3 ± 0.4 GPa, which is higher than that of polyamide 66 after water immersion (0.5–1.2 GPa), indicating the potential applicability of this composite as an alternative to polyamide 66.

Water resistance and mechanical properties of the acylated MFC–HAP composites are compared with those of the acylated starch–HAP composites and the acylated TCNF–HAP composites. For water resistance, both the acylated MFC–HAP composites and the starch–HAP composites exhibited low water absorption, while the acylated TCNF–HAP composites exhibited higher water absorption. The molded benzoylated MFC–HAP composite retained 70% of its initial modulus after water immersion, whereas the molded benzoylated TCNF–HAP composite exhibited only 2% of its initial modulus, indicating that the former possesses substantially higher water resistance. By integrating the findings of this study with prior research on acylated starch–HAP and acylated TCNF–HAP composites, it has been demonstrated that water absorption exceeding 10% leads to a substantial deterioration of mechanical properties upon immersion in water. For the fracture mechanism, both the acylated MFC–HAP composites and the acylated TCNF–HAP composites exhibited ductile fracture, while the acylated starch–HAP composites brittle fracture. A comparison of the three composites in terms of rigidity, toughness, and water resistance indicates that the benzoylated MFC–HAP composite exhibits the most superior overall performance.

## Conflicts of interest

There are no conflicts to declare.

## Data availability

All data included in this study are available upon request by contact with the corresponding author.

Supplementary information (SI): mechanical properties of the molded composites before and after immersion in water; the water absorption ratios, mole fractions of C, O, Ca and P of the fracture surface, TG traces of benzoylated MFC–HAP composites; photographs of the molded composite, benzoylated at 100 °C, after being immersed in water at room temperature for 24 h, SEM images of the fracture surface, the relative work of fracture *vs.* the water absorption ratio. See DOI: https://doi.org/10.1039/d5lp00282f.

## Acknowledgements

We thank Hiroyuki Matsumura, Tomohiro Hashizume, and Yohei Minami, Daicel Corporation, for supplying MFC samples and valuable discussion. This work was supported by a Grant-in-Aid for Scientific Research (22K05244) from the Japan Society for the Promotion of Science.

## References

1 K. P. Hickey, M. M. Macdonell and K. C. Picel, *Environ. Toxicol. Chem.*, 2025, **44**, 653.
2 S. Fang, X. Lyu, T. Tong, A. I. Lim, T. Li, J. Bao and Y. H. Hu, *Nat. Commun.*, 2023, **14**, 1203.
3 Y. Cho, P. T. T. Ninh, S. Hwang, S. Choe and J. Myung, *ACS Mater. Lett.*, 2025, **7**, 1563.
4 M. J. Olszta, X. Cheng, S. S. Jee, R. Kumar, Y. Kim, M. J. Kaufman, E. P. Douglas and L. B. Gower, *Mater. Sci. Eng., R*, 2007, **R58**, 77–116.
5 M. Granke, M. D. Does and J. S. Nyman, *Calcif. Tissue Int.*, 2015, **97**, 292–307.
6 S. V. Dorozhkin and M. Epple, *Angew. Chem., Int. Ed.*, 2002, **41**, 3130–3146.
7 H. P. Schwarcz, D. Abueidda and I. Jasiuk, *Front. Phys.*, 2017, **5**, 39, DOI: 10.3389/fphy.2017.00039.
8 D. Klemm, B. Heublein, H. Fink and A. Bohn, *Angew. Chem., Int. Ed.*, 2005, **44**, 3358–3393.
9 J. Deng, E. Zhu, G. Xu, N. Naik, V. Murugadoss, M. Ma, Z. Guo and Z. Shi, *Green Chem.*, 2021, **24**, 480.
10 C. W. Weyhrich, S. P. Petrova, K. J. Edgar and T. E. Long, *Green Chem.*, 2022, **25**, 106.
11 W. B. Costa, A. F. Félix Farias, E. C. Silva-Filho, J. A. Osajima, S. Medina-Carrasco, M. Del Mar Orta and M. G. Fonseca, *ACS Omega*, 2024, **9**, 30035, DOI: 10.1021/acsomega.4c02170.
12 W. Liu, N. Cheong, Z. He and T. Zhang, *J. Funct. Biomater.*, 2025, **16**, 127, DOI: 10.3390/jfb16040127.
13 A. N. Nakagaito and H. Yano, Nanocomposites based on cellulose microfibril. In Cellulose Nanocomposites: Processing, Characterization, and Properties, *ACS Symp. Ser.*, 2006, **938**, 151–168.
14 J. D. Currey, *Philos. Trans. R. Soc. London, Ser. B*, 1984, **304**, 509–518.
15 E. E. Wilson, A. Awonusi, M. D. Morris, D. H. Kohn, M. M. J. Tecklenburg and L. W. Beck, *Biophys. J.*, 2006, **90**, 3722–3731.
16 R. Hua, Q. Ni, T. D. Eliason, Y. Han, S. Gu, D. P. Nicolella, X. Wang and J. X. Jiang, *Matrix Biol.*, 2020, **94**, 95.
17 M. J. Duer, *J. Magn. Reson.*, 2015, **253**, 98, DOI: 10.1016/j.jmr.2014.12.011.
18 T. Azaïs, S. Von Euw, W. Ajili, S. Auzoux-Bordenave, P. Bertani, D. Gajan, L. Emsley, N. Nassif and A. Lesage, *Solid State Nucl. Magn. Reson.*, 2019, **102**, 2, DOI: 10.1016/j.ssnmr.2019.06.001.
19 P. Das, J. Malho, K. Rahimi, F. H. Schacher, B. Wang, D. E. Demco and A. Walther, *Nat. Commun.*, 2015, **6**, 5967.
20 A. Rimola, M. Corno, J. Garza and P. Ugliengo, *Philos. Trans. R. Soc., A*, 2012, **370**, 1478–1498.
21 P. Garnero, *Calcif. Tissue Int.*, 2015, **97**, 229.
22 L. Al-Qudsy, Y. Hu, H. Xu and P. Yang, *ACS Biomater. Sci. Eng.*, 2023, **9**, 2203.
23 G. Ulian, D. Moro and G. Valdrè, *Biomolecules*, 2021, **11**, 728.
24 J. Bradt, M. Mertig, A. Teresiak and W. Pompe, *Chem. Mater.*, 1999, **11**, 2694.

25 M. Kikuchi, T. Ikoma, S. Itoh, H. N. Matsumoto, Y. Koyama, K. Takakuda, K. Shinomiya and J. Tanaka, *Compos. Sci. Technol.*, 2004, **64**, 819–825.
26 J. Song, V. Malathong and C. R. Bertozzi, *J. Am. Chem. Soc.*, 2005, **127**, 3366–3372.
27 R. J. Coleman, K. S. Jack, S. Perrier and L. Grondahl, *Cryst. Growth Des.*, 2013, **13**, 4252–4259.
28 W. Fang, H. Zhang, J. Yin, B. Yang, Y. Zhang, J. Li and F. Yao, *Cryst. Growth Des.*, 2016, **16**, 1247–1255.
29 Y. Y. Hu, A. Rawal and K. Schmidt-Rohr, *Proc. Natl. Acad. Sci. U. S. A.*, 2010, **52**, 22425–22429.
30 Y. Okuda, R. Shigemasa, K. Hirota and T. Mizutani, *ACS Omega*, 2022, **7**, 12127–12137.
31 Y. Okuda, T. Mizutani, K. Hirota, T. Hayashi and K. Zinno, *ACS Sustainable Chem. Eng.*, 2021, **9**, 158–167.
32 Y. Okuda, Y. Aoyama, K. Hirota and T. Mizutani, *ACS Appl. Polym. Mater.*, 2022, **4**, 1666–1674.
33 Y. Okuda, E. Kido, K. Hirota and T. Mizutani, *ACS Appl. Polym. Mater.*, 2023, **5**, 8082–8088.
34 T. Heinze and T. Liebert, *Prog. Polym. Sci.*, 2001, **26**, 1689–1762.
35 M. A. Hubbe, O. J. Rojas, L. A. Lucia and M. Sain, *BioResources*, 2008, **3**, 929–980.
36 S. Vuoti, R. Talja, L. Johansson, H. Heikkinen and T. Tammelin, *Cellulose*, 2013, **20**, 2359–2370, DOI: 10.1007/s10570-013-9983-6.
37 S. Eyley and W. Thielemans, *Nanoscale*, 2014, **6**, 7764–7779, DOI: 10.1039/c4nr01756k.
38 Y. Wang, X. Wang, Y. Xie and K. Zhang, *Cellulose*, 2018, **25**, 3703–3731, DOI: 10.1007/s10570-018-1830-3.
39 A. Oberlintner, B. Likozar and U. Novak, *Carbohydr. Polym.*, 2021, **259**, 117742, DOI: 10.1016/j.carbpol.2021.117742.
40 Y. Okuda, R. Sasaki, E. Kido, K. Hirota and T. Mizutani, *ACS Omega*, 2024, **9**, 44457–44464.
41 A. F. Turbak, F. W. Snyder and K. R. Sandberg, *J. Appl. Polym. Sci.: Appl. Polym. Symp.*, 1983, **37**, 815–827.
42 H. Bai, F. Walsh, B. Gludovatz, B. Delattre, C. Huang, Y. Chen, A. P. Tomsia and R. O. Ritchie, *Adv. Mater.*, 2016, **28**, 50–56, DOI: 10.1002/adma.201504313.
43 J. E. Eastoe, P. Martens and N. R. Thomas, *Calcif. Tissue Res.*, 1973, **12**, 91–100.
44 S. O. Olusanya, S. M. Ajayi, K. O. Sodeinde, D. P. Fapojuwo, M. O. Atunde, A. E. Diduyemi, E. G. Olumayede and O. S. Lawal, *Polym. Bull.*, 2024, **81**, 1349, DOI: 10.1007/s00289-023-04756-y.
45 E. Jin, J. Guo, F. Yang, Y. Zhu, J. Song, Y. Jin and O. J. Rojas, *Carbohydr. Polym.*, 2016, **143**, 327.
46 K. S. Salem, N. K. Kasera, M. A. Rahman, H. Jameel, Y. Habibi, S. J. Eichhorn, A. D. French, L. Pal and L. A. Lucia, *Chem. Soc. Rev.*, 2023, **52**, 6417–6446.
47 R. H. Mehta, Physical constants of various polyamides: Poly[imino(1-oxohexamethylene)], (Polyamide 6)Poly(iminoadipoyl-iminohexamethylene)), (Polyamide 66) Poly (iminohexamethylene-iminosebacoyl), (Polyamide 610)Poly [imino(1-oxododecamethylene)], (Polyamide 12), in *Polymer Handbook*, ed. J. Brandrup, E. H. Immergut and E. A. Grulke, John Wiley and Sons, New York, 4th edn, 1998.
48 P. Le Gac and B. Fayolle, *Composites, Part B*, 2018, **153**, 256, DOI: 10.1016/j.compositesb.2018.07.028.
49 Y. Okuda, K. Hirota, T. Mizutani and Y. Aoyama, *Results Mater.*, 2019, **3**, 100035, DOI: 10.1016/j.rinma.2019.100035.
50 J. S. Nyman, A. Roy, X. Shen, R. L. Acuna, J. H. Tyler and X. Wang, *J. Biomech.*, 2006, **39**, 931–938.
51 J. A. Choren, S. M. Heinrich and M. B. Silver-Thorn, *J. Mater. Sci.*, 2013, **48**, 5103–5112.
52 K. K. Phani, *Am. Ceram. Soc. Bull.*, 1986, **65**, 1584–1586.
53 J. Kováčik, *J. Mater. Sci. Lett.*, 1999, **18**, 1007–1010.